Neurochemistry International 180 (2024) 105878

Contents lists available at ScienceDirect

Neurochemistry International

journal homepage: www.elsevier.com/locate/neuint

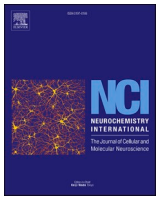

(Poly)phenol-rich grape and blueberry extract prevents LPS-induced disruption of the blood-brain barrier through the modulation of the gut microbiota-derived uremic toxins

Emily Connell [a], Gwénaëlle Le Gall [a], Simon McArthur [b], Leonie Lang [a], Bernadette Breeze [a], Matthew G. Pontifex [a], Saber Sami [a], Line Pourtau [c], David Gaudout [c], Michael Müller [a], David Vauzour [a,*]

[a] Norwich Medical School, Faculty of Medicine and Health Sciences, University of East Anglia, Norwich, NR4 7TJ, United Kingdom
[b] Institute of Dentistry, Faculty of Medicine & Dentistry, Queen Mary University of London, Blizard Institute, London, E1 2AT, United Kingdom
[c] Activ'Inside, Beychac et Caillau, France

A B S T R A C T

The dynamic protective capacity of (poly)phenols, attributed to their potent antioxidant and anti-inflammatory properties, has been consistently reported. Due to their capacity to alter gut microbiome composition, further actions of (poly)phenols may be exerted through the modulation of the microbiota-gut-brain axis. However, the underlying mechanisms remain poorly defined. Here, we investigated the protective effect of a (poly)phenol-rich grape and blueberry extract (Memophenol™), on the microbiota-gut-brain axis in a model of chronic low-grade inflammation (0.5 mg/kg/wk lipopolysaccharide (LPS) for 8 weeks). Dietary supplementation of male C57BL/6 J mice with Memophenol™ prevented LPS-induced increases in the microbe-derived uremia-associated molecules, indoxyl sulfate (IS) and trimethylamine *N*-oxide (TMAO). These changes coincided with shifts in gut microbiome composition, notably *Romboutsia* and *Desulfovibrio* abundance, respectively. In the brain, LPS exposure disrupted the marginal localisation of the endothelial tight junction ZO-1 and downregulated ZO-1 mRNA expression to an extent closely correlated with TMAO and IS levels; a process prevented by Memophenol™ intake. Hippocampal mRNA sequencing analysis revealed significant downregulation in regulatory pathways of neurodegeneration with Memophenol™ intake. These findings may indicate a novel protective role of the (poly)phenol-rich grape and blueberry extract on the endothelial tight junction component ZO-1, acting through modulation of gut microbial metabolism.

1. Introduction

(Poly)phenols are a diverse group of phytochemicals abundant in fruits, vegetables, and other plant-based foods. Renowned for their potent antioxidant and anti-inflammatory properties, (poly)phenols have been linked to the prevention of various chronic diseases, including cardiovascular diseases, cancers and neurodegenerative disorders, and are regarded as highly relevant modifiers of brain pathophysiology (Del Rio et al., 2013; Iqbal et al., 2023; Mutha et al., 2021; Ramis et al., 2020; Singh et al., 2008). Accordingly, dietary (poly)phenols are emerging as promising therapeutic strategies to promote healthy ageing due to their accessibility and the minimal side effects compared to pharmacological treatments.

One proposed mechanism linking dietary (poly)phenols to the brain is through the modulation of a 'microbiota-gut-brain' axis, a bidirectional signalling pathway connecting the gut and the brain that is modulated by the gut microbiome (Láng et al., 2024). Recent pre-clinical and clinical evidence has revealed the significance of (poly)phenols on gut microbiota composition, promoting the growth of beneficial bacteria and suppressing pathogenic species (Láng et al., 2024; Mithul Aravind et al., 2021; Romo-Vaquero et al., 2022; Song et al., 2021). Modulation of the gut microbiome has the capability to alter numerous microbial-derived metabolite, neuroendocrine, autonomic and neuroimmune pathways, directly and indirectly influencing brain function (Chakrabarti et al., 2022; Connell et al., 2022).

Grapes and blueberries are rich sources of (poly)phenols. Blueberries, containing high concentrations of anthocyanins (Ma et al., 2018), and grapes, consisting of flavonoids (flavan-3-ols, flavonols, anthocyanins and flavones), and non-flavonoids (phenolic acids and stilbenes) (Garrido and Borges, 2013), have been studied in both human (Krikorian et al., 2010a, 2010b) and rodent models (Dal-Pan et al., 2017; Rendeiro et al., 2012; Sarkaki et al., 2007; Shukitt-Hale et al., 2006) for their potential to enhance cognitive performance and protect against cognitive decline. Supplements containing high concentrations of (poly)

* Corresponding author.
E-mail address: D.Vauzour@uea.ac.uk (D. Vauzour).

https://doi.org/10.1016/j.neuint.2024.105878
Received 24 June 2024; Received in revised form 9 September 2024; Accepted 7 October 2024
Available online 9 October 2024

phenols are increasingly popular as a convenient method to boost the intake of beneficial compounds, which may enhance cognitive function (Troppmann et al., 2002). Memophenol™, a patented (WO/2017/072, 219) (poly)phenol-rich blueberry and grape extract, has been reported to prevent age-related spatial memory deficits in aged mice (Bensalem et al., 2016) and to improve recognition memory in 3xTg-AD mice, a model of Alzheimer's disease (Dal-Pan et al., 2017). Furthermore, consumption of Memophenol™ was reported to improve cognitive capabilities in healthy young adults (Philip et al., 2019), elderly individuals (Bensalem et al., 2019) and older adults with mild cognitive impairment (Lopresti et al., 2023). However, whether these effects are due to modulation of the microbiota-gut-brain axis remains unknown.

In this study, we present for the first time the effect of a (poly)phenol-rich grape and blueberry extract, Memophenol™, on the microbiota-gut-brain axis; exploring its effect on gut microbiota composition, quantifying key circulatory microbial-derived metabolites associated with cognitive health (Connell et al., 2022) and underlying neuronal gene expression changes in the brain, in the context of an LPS model of chronic low-grade inflammation.

2. Materials and methods

2.1. Study approval

All experimental procedures and protocols performed were reviewed and approved by the Animal Welfare and Ethical Review Body (AWERB) of the University of East Anglia and were conducted in accordance with the United Kingdom Animals (Scientific Procedures) Act, 1986 Amendment Regulations, 2012) under project licence PPL80/2533. Reporting of the study outcomes complies with the ARRIVE (Animal Research: Reporting of In Vivo Experiments) guidelines (Sert et al., 2020).

2.2. Overview of experimental procedure

Thirty male C57BL/6 J mice sourced from Charles River (Margate, UK) were maintained in individually ventilated cages (n = 5 per cage), within a controlled environment (21 ± 2 °C; 12 h light/dark cycle; light from 7:00 a.m.). Mice were fed *ad libitum* on a standard diet (RM3-P; Special Diet Services (SDS, Horley UK)) up to the age of 10 weeks, ensuring normal development and stabilisation of the microbiota. Mice were subsequently divided into three groups ($n = 10$ per group): 1) the control group fed the standardised AIN93-M diet with a sham injection of saline, 2) the lipopolysaccharide (LPS) group formed of mice fed the standardised AIN93-M with LPS administration or 3) the LPS + Memophenol™, a (poly)phenol-rich grape and blueberry extract (Supplementary Table S1), group consisting of mice consuming the Memophenol™ diet (Activ'Inside, Beychac-et-Caillau, France) with LPS administration, for eight weeks. The Memophenol™ diet consisted of the background AIN93-M supplemented with 879 mg kg−1 diet of Memophenol™ (see Supplementary Table S2 for full dietary composition). Diets were prepared by Research Diet Inc. (New Brunswick, USA) to comply with animal nutrition requirements. Chronic low-grade inflammation was initiated upon switching of the diets and was induced through weekly intraperitoneal injections (IP) of 0.5 mg kg−1 LPS (*Escherichia coli* O111:B4, Merck Life Science, UK) for 8 weeks as described previously (Hoyles et al., 2021; Pontifex et al., 2022) or a sham injection consisting of 0.9% saline to control mice. At the end of the experiments, 5-month-old animals were sedated with isoflurane (1.5%) in 70% nitrous oxide/30% oxygen mix and transcardially perfused with ice-cold 0.9% saline containing 10 UI heparin (Sigma-Aldrich, UK). Whole blood was allowed to clot in ice for 30 min before isolating the serum by centrifugation at 4,000 g for 10 min. Brains were rapidly removed, halved, snap-frozen and stored at −80 °C until biochemical, immunohistochemical and transcriptomic analyses. Additionally, caeca were removed, weighed and contents were extracted. Samples were then snap-frozen in liquid nitrogen and stored at −80 °C until further analysis.

2.3. Microbial DNA extraction and 16S rRNA amplicon sequencing

Microbial DNA was isolated from approximately 50 mg of caecal content from $n = 6$ randomly selected animals and using the QIAamp PowerFecal Pro DNA Kit (Qiagen, Manchester, UK) as per the manufacturer's instructions. DNA quantity was assessed using a Nanodrop 2000 Spectrophotometer (Fisher Scientific, UK). Quality assessment was performed by agarose gel electrophoresis to detect DNA integrity, purity, fragment size and concentration. The 16 S rRNA amplicon sequencing of the V3–V4 hypervariable region was performed with an Illumina NovaSeq 6000 PE250. Sequence analysis was performed by Uparse software (Uparse v7.0.1001) (Wang et al., 2007), using all the effective tags. Sequences with ≥97% similarity were assigned to the same OTUs. A representative sequence for each OTU was screened for further annotation. For each representative sequence, Mothur software was performed against the SSUrRNA database of SILVA Database 138 (Quast et al., 2013). OTUs abundance information was normalised using a standard sequence number corresponding to the sample with the least sequences and transformed using centered log ratio (CLR). Alpha diversity was assessed using both Chao1 and Shannon H diversity index whilst beta diversity was assessed using Bray–Curtis. Statistical significance was determined by Kruskal–Wallis or Permutational Multivariate Analysis of Variance (PERMANOVA). Comparisons at the genus level were made using classical univariate analysis using Kruskal–Wallis combined with a false discovery rate (FDR) approach used to correct for multiple testing.

2.4. LC-MS/MS

Liquid chromatography with tandem mass spectrometry (LC-MS/MS) was conducted to gain insight into possible shifts in the production of bioactive serum metabolites and targeted metabolites previously associated with cognitive health, including bile acids, tryptophan, trimethylamine *N*-oxide (TMAO), *p*-cresol and its derivatives (Connell et al., 2022). Serum samples (80 μL) were diluted with methanol at a ratio of 1:10 (*v*/*v*) and placed on dry ice for 10 min. Samples were then centrifuged (5 min, 16,000×*g* at room temp), supernatants filtered using a 0.45 μm PTFE syringe filter and evaporated to dryness using a Savant™ SpeedVac™ High-Capacity Concentrator (Thermofisher, UK). Dried samples were resuspended in either 50 μL of methanol with the addition of 15 μL of lithocholic acid-d4 and cholic acid-d4 at 50 μg/mL for the detection of bile acids, 50 μL water with TMA-d9 *N*-oxide, TMA $^{13}C^{15}N$ hydrochloride at 50 μg/mL for the detection of TMAO/TMA/-choline or 50 μL water with 15 μL of L-methionine-3, 3, 4, 4 d^4 and *p*-toluenesulfonic acid at 50 μg/mL for the detection of tryptophan and *p*-cresol metabolites respectively. All internal standards were supplied from Thermofisher, UK. Samples were analysed using Waters Acquity UPLC system and Xevo TQ-S Cronos mass spectrometer with MassLynx 4.1 software. For the detection of bile acids, the electrospray ionisation (ESI) operated in negative mode and chromatographic separations were performed with a Supelco Ascentis Express C18 column (150 × 4.6 mm, 2.7 μM). A binary gradient of eluent A (10 mM ammonium acetate, 0.1% formic acid, water) and eluent B (10 mM ammonium acetate, 0.1% formic acid, methanol) ran at a constant rate of 0.6 mL/min. For the quantification of TMAO, TMA and choline, ESI operated in positive mode. Chromatographic separation was achieved using an Ethylene Bridged Hybrid (BEH) Amide (150 × 2.1 mm, 1.7 μM) and 0.5 mL/min using eluent A (10 mM ammonium formate, 0.2% formic acid, 50% acetonitrile) and eluent B (10 mM ammonium formate, 0.2% formic acid, 95% acetonitrile). For the detection of tryptophan and *p*-cresol related metabolites, ESI operated in positive mode using an Acquity UPLC BEH C18 1.7 μM (2.1 × 50 mm) column. A binary gradient of eluent A (0.1% formic acid, water) and eluent B (0.1% formic acid,

methanol) held a constant flow rate of 0.3 mL/min. Chromatogram peak analysis was performed by the accompanying Waters® TargetLynx ™ application manager. Three samples (one from each group) were excluded due to being considered outliers based on their low intensities in total signal levels (Moreno-Torres et al., 2021). These outliers were identified through an assessment of the signal intensity across the samples to ensure the robustness and reliability of the dataset. Gradients for all three methods are described elsewhere (Connell et al., 2024).

2.5. Immunofluorescent staining

Coronal brain cryosections (20 μm) containing the hippocampus were processed from the left hemisphere of snap-frozen brain samples. Cryosections were mounted onto glass slides before being fixed in 4% formaldehyde in PBS for 15 min. Sections were washed in Tris-buffered saline (TBS; 50 mM Tris base, 150 mM NaCl, pH 7.4) containing 0.05% Triton X-100 for 10 min, followed by blocking with TBS containing 10% normal goat serum and incubated with the primary antibody for 1 h at room temperature (polyclonal rabbit anti-mouse zonula occludens-1 (ZO-1), 1:100, Thermofisher Scientific, UK), diluted in TBS containing 0.1% normal goat serum. Nuclei were counterstained with DAPI (Sigma–Aldrich, UK). Images were collected from the hippocampus of each mouse using a Direct Fluorescence Leica Ctr 5000 Microscope at ×10 magnification. Image analysis was performed using ImageJ (version 1.53) software (NIH, Washington DC, USA).

2.6. RNA isolation and sequencing

Total RNA was isolated from hippocampi ($n = 4$, randomly selected from each group) using the Qiazol reagent (Qiagen, UK). Messenger RNA was then purified from total RNA using poly-T oligo-attached magnetic beads. After fragmentation, the first strand cDNA was synthesized using random hexamer primers, followed by the second strand cDNA synthesis using either dUTP for a directional library or dTTP for non-directional library (Parkhomchuk et al., 2009). The libraries were checked with Qubit and real-time PCR for quantification and bioanalyzer for size distribution detection. Quantified libraries were pooled and sequenced on Illumina platforms, according to effective library concentration and data amount. Raw data (raw reads) of FASTQ format were first processed through in-house Perl scripts. All the downstream analyses were based on clean data with high quality. The index of the reference genome was built using Hisat2 v2.0.5 (Mortazavi et al., 2008) and paired-end clean 1 reads were aligned to the reference genome using Hisat2 v2.0.5. FeatureCounts v1.5.0-p3 was used to count the reads numbers mapped to each gene (Liao et al., 2014). Then FPKM of each gene was calculated based on the length of the gene and read count mapped to this gene.

2.7. qRT-PCR

RNA was prepared as outlined above. Two μg of total RNA was treated with DNase I (Invitrogen, UK) and used for cDNA synthesis using Invitrogen™ Oligo (dT) primers and *M*-MMLV reverse transcriptase. Quantitative real-time PCR (qRT-PCR) reactions were performed using SYBR green detection technology on the Applied Biosystems QuantStudio 5 Real-Time PCR system (Life Technologies). Results are expressed as relative fold change in LPS and LPS + Memophenol™ in comparison to the control group, which has been scaled to the average across all samples per target gene and normalised to the geometric mean of three reference genes, TATA-box binding protein (*Tbp*), glyceraldehyde-3-phosphate dehydrogenase (*Gapdh*) and hypoxanthine phosphoribosyltransferase 1 (*Hprt 1*). The primer sequences are given in Supplementary Table S3.

2.8. Statistical analysis

Data analysis was performed in GraphPad Prism version 9.5.1 (GraphPad Software, CA, USA). All data are presented as means ± standard error of the means (SEM) unless otherwise stated. After identifying outliers using the ROUT method (q = 1%), data were checked for normality/equal variances using the Shapiro–Wilk test. For analysis of dietary intervention, a one-way ANOVA or Kruskal Wallis test was used followed by Tukey or Dunns's multiple comparison depending on the normality of data. *P*-values of less than 0.05 were considered statistically significant.

Statistical analysis of metabolomics data was carried out using Metaboanalyst 5.0 (Pang et al., 2022). Partial Least-Squares Discriminant Analysis (PLS-DA) was employed to illustrate the clustering of different metabolites across groups. Univariate Analysis was carried out by one-way ANOVA, followed by Tukey HSD. Dendrogram and heatmaps were created with Spearman and Ward. Procrustes analysis (PA), investigating the congruence of the metabolomics and microbiome data, was conducted using M2IA (Ni et al., 2020). Correlation network analysis was performed to uncover complex relationships between microbial-derived metabolites and neuronal gene expression data. Correlations were calculated using Spearman rank-order correlation coefficient. Significant correlations ($R > 0.5$; $p < 0.05$) were used to construct a network in which nodes represent significantly modulated metabolites ($p < 0.05$) and edges represent significant correlations. The network was visualised using Omics Analyst (Zhou et al., 2021). Modules were constructed using the label propagation algorithm. Functional enrichment analysis of network clusters was performed using KEGG pathway analysis to identify overrepresented biological processes and pathways. All other correlation analyses were conducted using Spearman's rank-order correlation analysis.

3. Results

3.1. Chronic low-dose LPS exposure and Memophenol™ supplementation does not impact body weight

Although body weight significantly increased over the 8-week period ($F(7, 189) = 55.67$; $P < 0.0001$), this was comparable across all experimental groups ($F(2, 27) = 0.1197$; $p = 0.89$) (Fig. 1A). Overall body weight gain throughout the experiment did not differ between groups ($F(2, 27) = 0.6681$; $p = 0.5220$) (Fig. 1B). There was no significant difference in mean food intake throughout the study with mice consuming on average 3.21 ± 0.18 g per day per mouse, providing the animals with 97.2 ± 5.9 mg per kg bw per day of Memophenol™. Using allometric scaling based on body surface area (Nair and Jacob, 2016), this dose equates to 472.2 ± 28.5 mg per day human equivalent dose for a person of 60 kg.

3.2. Chronic low-dose LPS exposure and Memophenol™ supplementation display modest shifts in intestinal microbiota and metabolism

The impact of LPS and LPS + Memophenol™ on the gut microbiome was investigated using 16 S rRNA amplicon sequencing. Alpha diversity was measured using Chao1 ($F(2, 15) = 2.16$; $p = 0.15$) and Shannon H ($F(2, 15) = 0.15$; $p = 0.86$) index and suggested no significant differences between treatment groups (Fig. 2A). Conversely, PCoA as measured by Bray-Curtis distances, suggested beta diversity was significantly altered between groups (PERMANOVA F-value = 1.73; R-squared = 0.21; $p = 0.001$) (Fig. 2B). Pairwise comparisons demonstrated this shift was most significant between control and LPS ($p = 0.005$, FDR $q = 0.015$; Supplementary Table S4). Conversely, the shift between LPS and LPS + Memophenol™ was more subtle ($p = 0.096$, FDR $q = 0.186$). At the genus level, seven genera were found to be significantly altered ($q < 0.05$) between treatment groups, including *Erysipelotrichaceae* ($q = 0.016$), *Muribaculum* ($q = 0.016$),

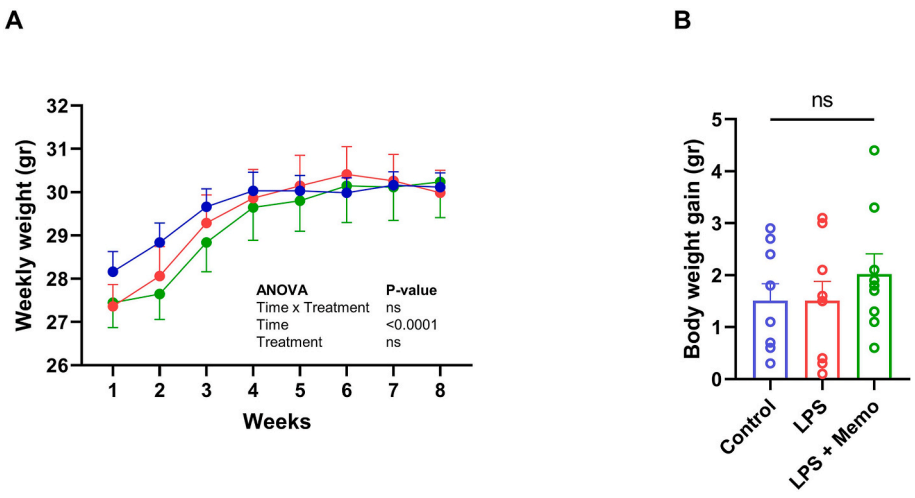

Fig. 1. Administration of LPS (0.5 mg per kg bw per week) and LPS + Memophenol™ supplementation does not significantly impact body weight. (A) Average weekly weight of mice from each group, which although increased significantly over the course of the experiment, did not significantly differ between groups. (B) The total average weight mice gained from each group during the experiment did not significantly differ. Error bars represent SEM. ns; no significant.

Rikenellaceae_RC9_group ($q = 0.017$), *Butyricicoccus* ($q = 0.017$), *Alistipes* ($q = 0.027$), *Lachnospiraceae A2* ($q = 0.030$), *Desulfovibrio* ($q = 0.03$), *Muribaculaceae* ($q = 0.032$) and *Romboutsia* ($q = 0.034$) (Supplementary Table S5). *Muribaculum* abundance was significantly decreased by LPS in comparison to control. However, the abundance was partially restored by Memophenol™ supplementation (Fig. 2C). *Eubacterium_brachy_group* and *Romboutsia* abundance was also decreased by LPS but was significantly increased in the LPS + Memophenol™ group (Fig. 2D–E). LPS also induced significant increases in *Desulfovibrio* and the ratio of Firmicutes: Bacteroidota ($p < 0.05$) in comparison to controls (Fig. 2F–G). However, Memophenol™ supplementation partially restored levels.

Partial Least-Squares Discriminant Analysis (PLS-DA) showed a shift in metabolomic profiles between the treatment groups, suggesting a change in metabolic response between control, LPS and LPS + Memophenol™ groups (Fig. 3A). This was confirmed by hierarchical clustering highlighting relative changes in the abundance of 38 metabolites (Fig. 3B). The concentration of four metabolites, trimethylamine *N*-oxide (TMAO; $F(2, 24) = 6.96$, $P = 0.004$), indoxyl sulfate (IS; $F(2, 24) = 5.12$; $P = 0.014$), *p*-cresol sulfate (PCS; $F(2, 24) = 4.68$; $P = 0.019$) and *p*-cresol glucuronide (PCG; $F(2, 24) = 5.36$; $P = 0.012$) were significantly modulated between the three groups ($p < 0.05$). TMAO and IS were significantly increased in LPS in comparison to control. However, supplementation with Memophenol™ prevented the LPS-induced increase (Fig. 3C). PCS and PCG were significantly decreased in LPS + Memophenol™ in comparison to LPS and PCG were also significantly decreased from controls (Fig. 3D). Choline ($F(2, 24) = 2.62$; $P = 0.093$), indole-3-lactic acid (ILA; $F(2, 24) = 5.41$; $P = 0.056$), tryptophan ($F(92, 24) = 2.90$; $P = 0.074$) and indole-3-acetic acid (IAA; $F(2, 24) = 2.85$; $P = 0.078$) were modulated near statistical significance. A full list of metabolite concentrations is provided in Supplementary Table S6.

Procrustes analysis evaluated the global similarity between metabolome and microbiome datasets. Control and LPS groups displayed significant congruence of the datasets ($R = 0.6$, $p = 0.04$) and LPS + Memophenol™ and LPS groups suggested near significant similarity ($R = 0.55$, $p = 0.08$) (Supplementary Fig. S1). Conversely, control and LPS + Memophenol™ groups were less congruent ($R = 0.46$, $p = 0.28$). Spearman rank correlation analysis highlighted a significant relationship between metabolites modulated between treatment groups ($p < 0.05$) and microbial genera (Fig. 3E). Interestingly, TMAO positively correlated with *Desulfovibrio,* a choline to trimethylamine (TMA) converter, (Craciun and Balskus, 2012), while IS negatively correlated with *Romboutsia*, a bacterium associated with tryptophan metabolism via the kynurenine pathway (Vazquez-Medina et al., 2024) (Supplementary Fig. S2).

3.3. Chronic low-dose LPS exposure disrupts the endothelial tight junction, ZO-1, which is diminished by Memophenol™ supplementation

Blood-brain barrier (BBB) permeability is underpinned by inter-endothelial tight junctions that interact with the actin cytoskeleton and can be disrupted by chronic low-grade inflammation (Gan et al., 2023). As such, we examined the effect of the treatment groups on the key tight junction component zonula occludens-1 (ZO-1). In comparison with the control group, LPS disrupted the marginal localisation of ZO-1, an effect not seen after treatment with Memophenol™ (Fig. 4A). This was supported by a significant reduction in ZO-1 intensity in the LPS group in comparison to controls that was mitigated by the addition of Memophenol™ (Fig. 4B) and downregulation of mRNA expression of the gene encoding the ZO-1 protein, tight junction protein 1 (*Tjp1*), under LPS in comparison to control ($p = 0.046$), which was subsequently increased by Memophenol™ ($p = 0.005$) (Fig. 4C). Changes in *Tjp1* expression were found to negatively correlate with circulatory TMAO ($R = -0.88$; $p < 0.001$) and IS ($R = -0.45$; $p = 0.039$) concentrations (Supplementary Table S7). As IS and TMAO levels were significantly modulated between treatment groups, with LPS-induced increases prevented by Memophenol™ intake, these correlations were of particular interest (Fig. 4D). Further markers of BBB permeability, including occludin ($F(2,9) = 1.20$; $p = 0.35$), annexin A1 ($F(2,9) = 2.02$; $p = 0.18$) and claudin 5 ($F(2,9) = 1.07$; $p = 0.38$), were not significantly modulated between treatment groups (Supplementary Fig. S3).

3.4. Memophenol™ supplementation prevented the LPS-induced increase in pathways of neurodegeneration, which was associated with changes in indoxyl sulfate

To examine the potential neuroprotective mechanisms of Memophenol™ against LPS-induced low-grade inflammation, RNA sequencing analysis was conducted on the hippocampal brain region. Differentially expressed genes (DEG) were screened between pairwise comparisons of the three groups [(1) control SHAM vs. LPS, (2) control SHAM vs. LPS + Memophenol™, (3) LPS + Memophenol™ vs. LPS ($p < 0.05$)] (Fig. 5A). A total of 2,730 genes were differentially expressed between groups, with 20 genes similarly differentially expressed between all three pairwise comparisons. Hierarchical clustering analysis displayed the expression of significant DEGs between all groups (Fig. 5B). Correlation network analysis revealed significant associations

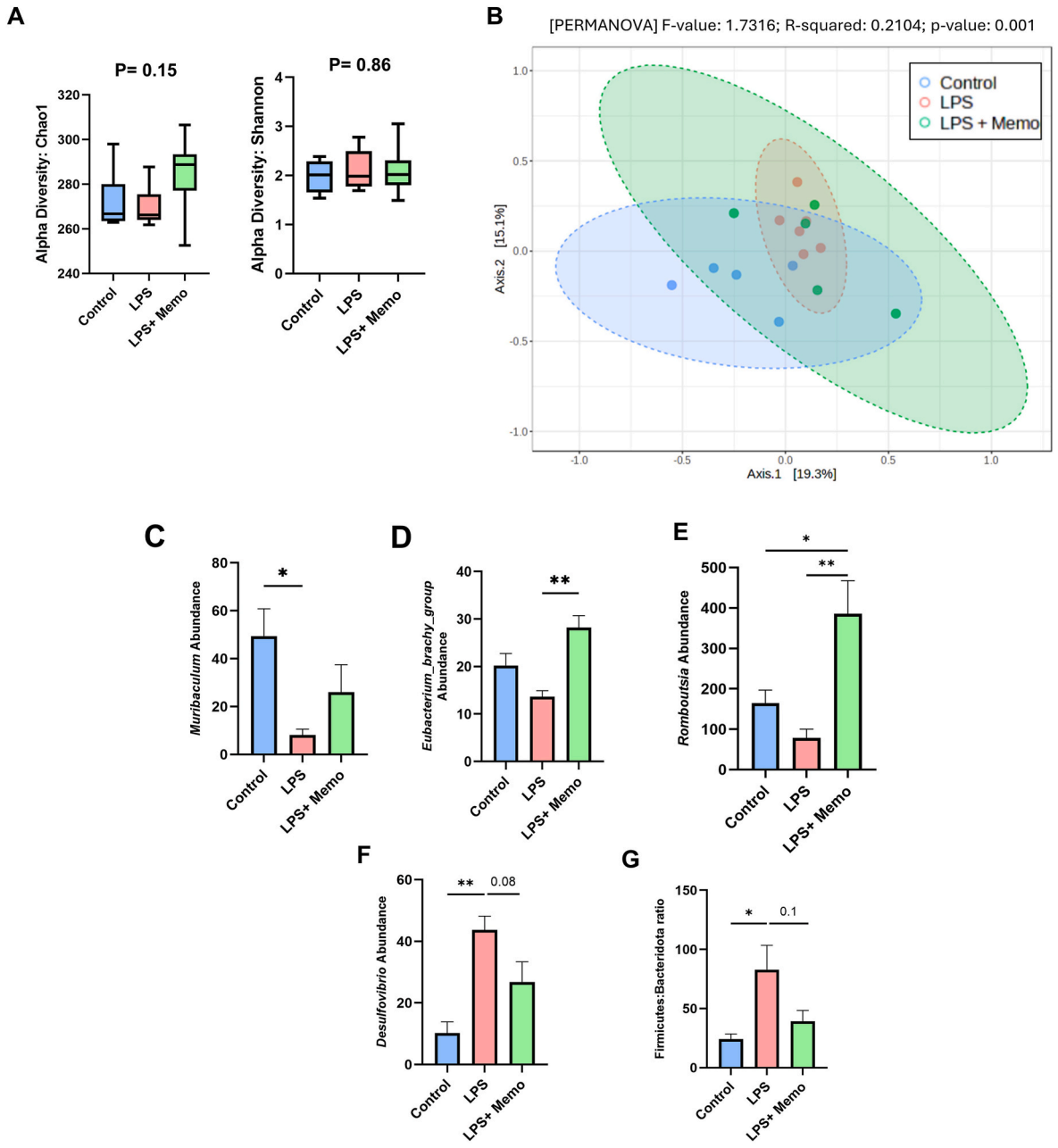

Fig. 2. Administration of LPS and LPS + Memophenol™ altered beta, but not alpha diversity of the gut microbiome. (A) Alpha diversity as measured by Chao1 and Shannon H index was not significantly modulated between groups. (B) Beta diversity as measured by Bray-curtis; p-value generated from PERMANOVA. Abundance of bacteria that are modulated by LPS and are in part restored by Memophenol™, including *Muribaculum* (C), *Eubacterium_brachy_group* (D), *Romboutsia* (E), *Desulfovibrio* (F) and Firmicutes: Bacteridota ratio (G) in control, LPS and LPS + Memophenol™.

between circulatory microbial-derived metabolites and neuronal gene expression (Fig. 5C). Significant modulation of TMAO between groups correlated with 63 genes in the brain, including a negative correlation with 22 genes and a positive correlation with 41 genes (Supplementary Table S8). These genes were associated with modulation of cysteine and methionine metabolism ($p = 0.006$), selenocompound metabolism ($p = 0.037$), EGFR tyrosine kinase inhibitor resistance ($p = 0.039$), one carbon pool by folate ($p = 0.041$), maturity onset diabetes of the young ($p = 0.042$) and mannose type *O*-glycan biosynthesis ($p = 0.049$). PCG correlated with 451 genes, including 163 negatively correlated and 288 positively correlated. These genes were associated with oxidative phosphorylation ($p < 0.0001$), glutamatergic synapse ($p < 0.0001$), neurotrophin signalling ($p = 0.002$), ABC transporters ($p = 0.002$), pentose phosphate pathway ($p = 0.002$) and fructose and mannose metabolism ($p = 0.003$). PCS correlated with 268 genes, 107 were negatively correlated and 161 were positively correlated (Supplementary Table S9). These genes were mostly associated with pyruvate metabolism ($p = 0.002$), renin-angiotensin system ($p = 0.003$), fatty acid elongation ($p = 0.017$), neurotrophin signalling pathway ($p = 0.018$), calcium signalling pathway ($p = 0.047$) and cysteine and methionine metabolism ($p = 0.049$). IS concentrations were correlated with 52 genes, including 20 genes negatively correlated and 32 genes positively correlated (Supplementary Table S10). These genes were associated with hematopoietic cell lineage ($p = 0.0001$), complement and coagulation cascades ($p = 0.009$), graft-versus-host disease ($p = 0.009$), Notch signalling pathway ($p = 0.001$), D-glutamine and D-glutamate metabolism ($p = 0.01$) and pathways of neurodegeneration ($p = 0.01$). The correlation between IS and pathways of

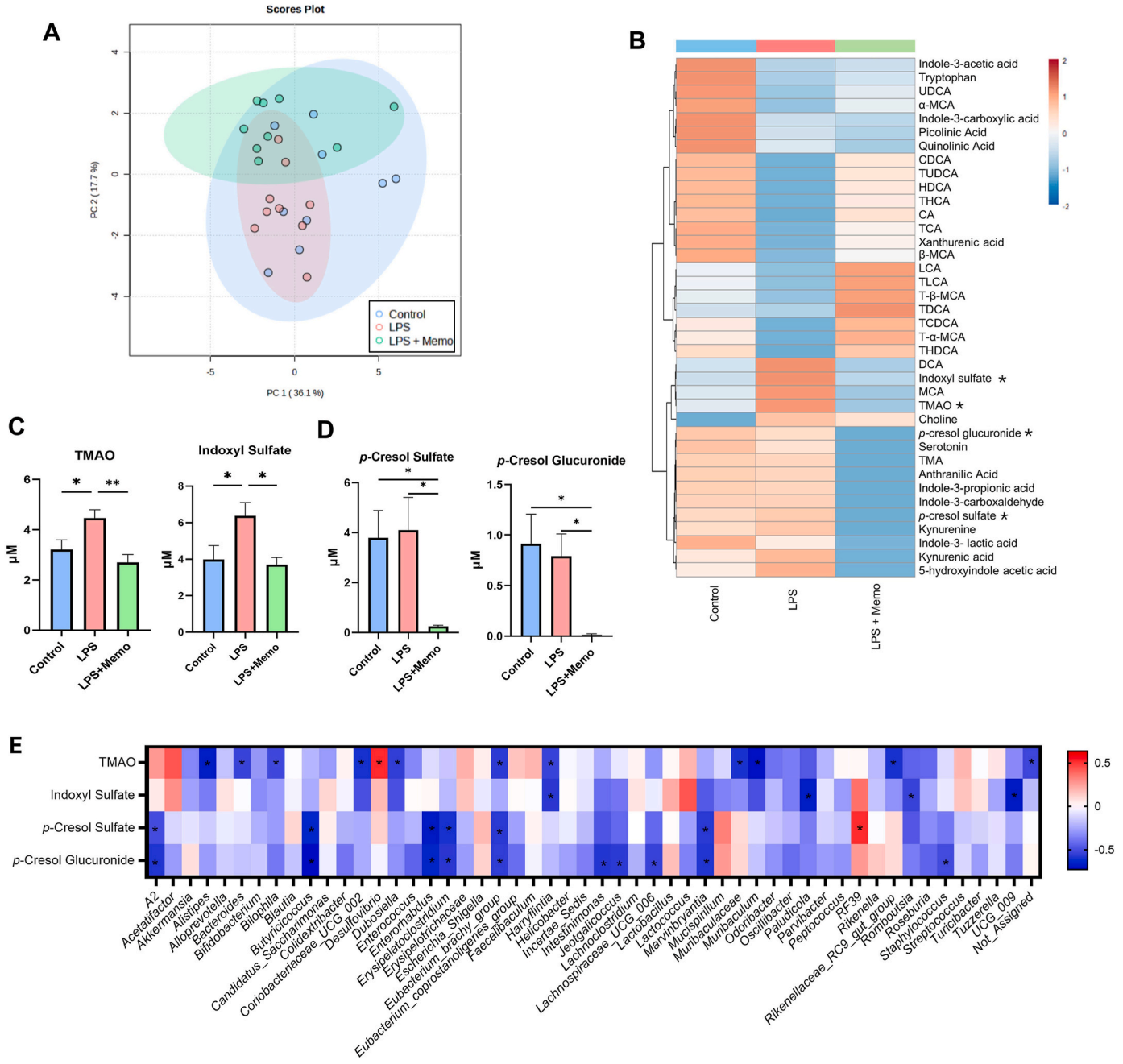

Fig. 3. Microbial-derived uremic toxins were significantly modulated between groups and associated with changes in the gut microbiome composition. (A) Partial least squares-discriminant analysis (PLS-DA) plot of the metabolomic profiles. (B) Heatmap displaying changes in concentrations of metabolites between the groups, with hierarchical clustering. * = $p < 0.05$ between groups. (C) Concentrations of significantly modulated ($p < 0.05$) uremic toxins TMAO and indoxyl sulfate are increased under LPS challenge but restored with Memophenol™ supplementation. (D) Concentrations of significantly modulated ($p < 0.05$) cresol metabolites between treatment groups (*p*-cresol sulfate (PCS) and *p*-cresol glucuronide (PCG)). *$p < 0.05$, **$p < 0.01$. (E) Spearman rank correlation analysis between significantly modulated metabolites and the gut microbiome genera. * = $p < 0.05$. Red = positive correlation. Blue = negative correlation. (For interpretation of the references to colour in this figure legend, the reader is referred to the Web version of this article.)

neurodegeneration was of particular interest as these genes may provide insight into the mechanisms associating IS and the observed changes in ZO-1 expression. This pathway consisted of significant modulation of inducible nitric oxide synthase (*iNOS/Nos2*) and caspase-3 (*Casp3*), which were both upregulated by LPS in comparison to control, but the increase was prevented by Memophenol™ supplementation (Fig. 5D). NOS2 is a known producer of nitric oxide (NO), a mediator implicated in neuroinflammatory processes and neurodegeneration (Colton et al., 2006) and caspase-3 is a critical executor of apoptosis (Brentnall et al., 2013). RNA sequencing also highlighted a significant decrease in the expression of the ATP-binding cassette transporter subfamily G member 2 (*Abcg2*), an exporter of IS (Takada et al., 2018), under LPS challenge which was subsequently recovered by Memophenol™ supplementation (Fig. 5E). Importantly, RNA sequencing results did not significantly differ from qPCR results on *Tjp1* expression and a randomly selected differentially expressed gene; *Slco1a4* (Supplementary Fig. S4).

4. Discussion

Diet represents one of the largest factors influencing intestinal

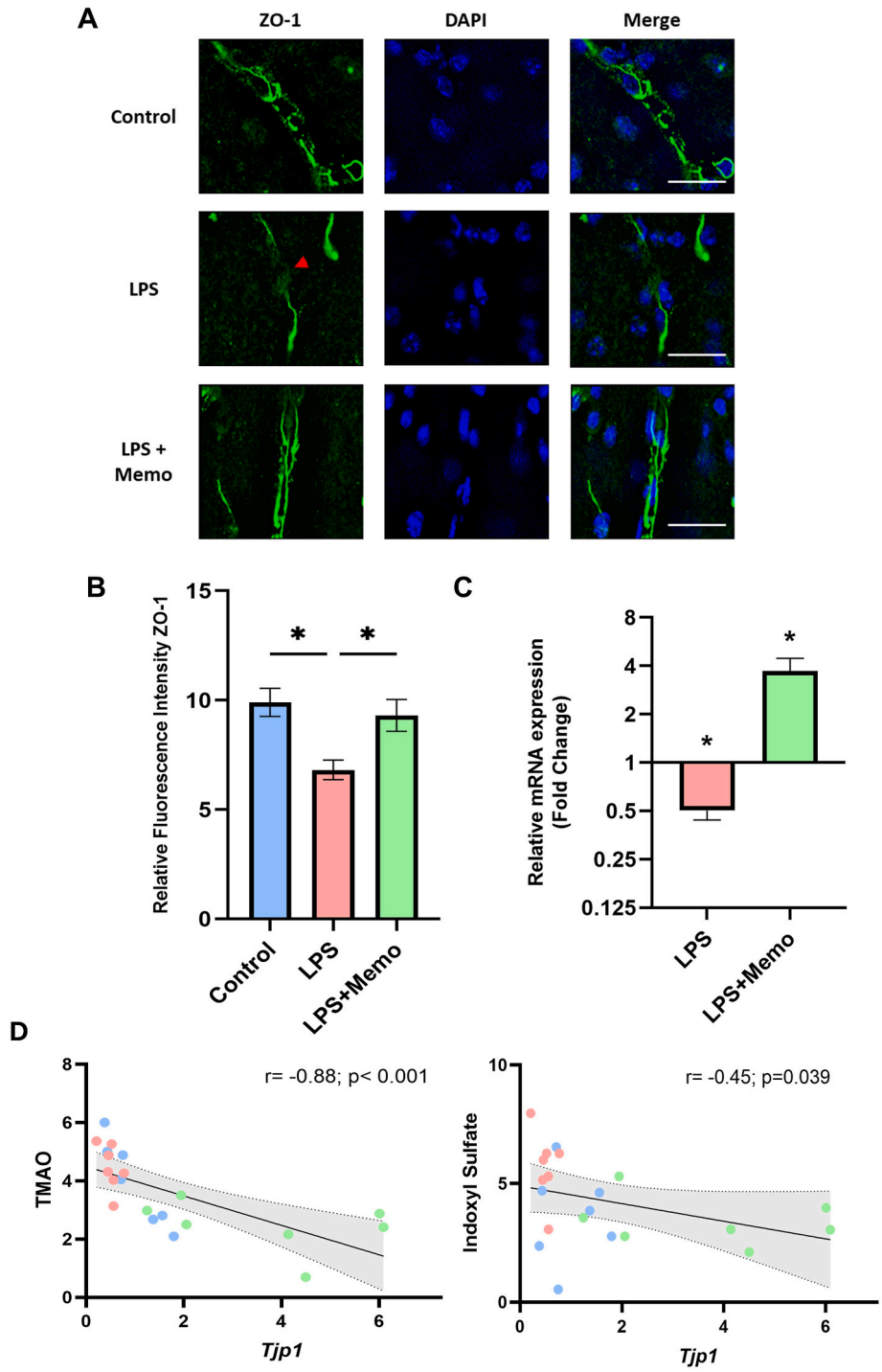

Fig. 4. Memophenol™ recovers LPS-induced decreases in ZO-1. (A) Representative images of expression of the tight junction component zona occludens-1 (ZO-1). Red arrowhead indicates an example site of ZO-1 disruption. Scale bar represents 10 μm. Images are representative of at least four independent experiments. (B) Relative fluorescence intensity of ZO-1 images. (C) Fold change of *Tjp1* relative mRNA expression in LPS and LPS + Memophenol™ from control group. * = significant change from control group. (D) Correlation analysis between TMAO and indoxyl sulfate concentrations and *Tjp1* expression. Blue points represent control group, red points signify LPS and green points display LPS + Memophenol™. (For interpretation of the references to colour in this figure legend, the reader is referred to the Web version of this article.)

microbiota activity, offering a promising therapeutic avenue to modulate many aspects of human health, including the CNS, via modulation of the microbiota-gut-brain axis (Moles and Otaegui, 2020). Here, we investigated the effectiveness of a (poly)phenol-rich grape and blueberry extract, Memophenol™, in countering the harmful effects of chronic LPS-induced low-grade inflammation. Our results highlight a novel protective effect of Memophenol™, significantly reducing adverse effects of LPS on gut-derived uremic toxins, IS and TMAO, indicating modulation of metabolic pathways related to microbial or biosynthetic metabolism. Indeed, TMAO and IS concentrations correlated with *Desulfovibrio* and *Romboutsia* abundance, respectively. LPS also induced disruption of the endothelial tight junction protein, ZO-1. Concentrations of IS and TMAO were inversely correlated with the modulation of ZO-1 expression, with changes in IS positively associated with

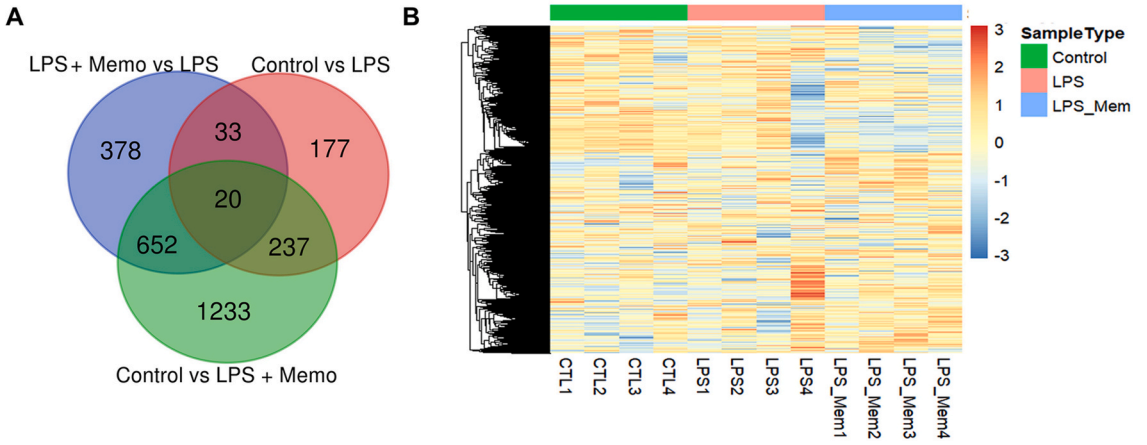

C

KEGG Pathways	Hits	P.Value
Cysteine and methionine metabolism	2	0.00568
Selenocompound metabolism	1	0.0367
EGFR tyrosine kinase inhibitor resistance	7	0.0394
One carbon pool by folate	1	0.041
Maturity onset diabetes of the young	2	0.0421
Mannose type *O*-glycan biosynthesis	1	0.0494

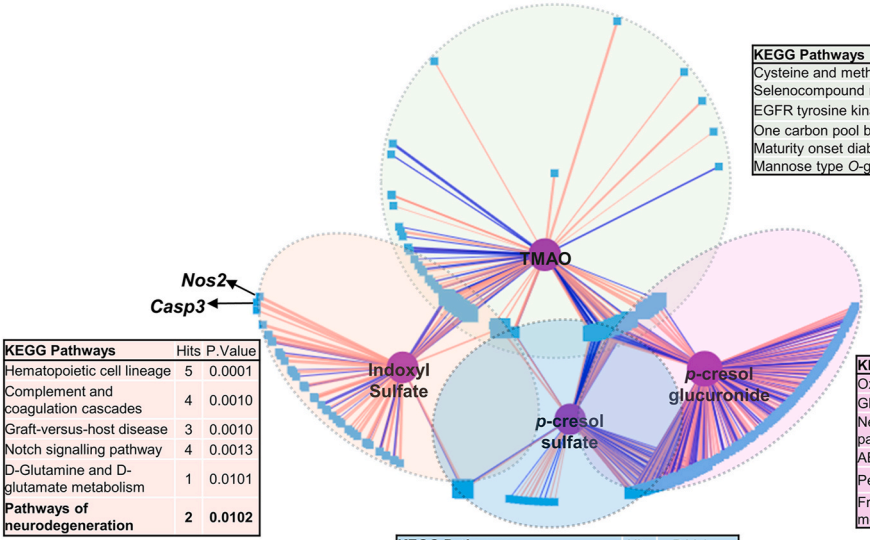

KEGG Pathways	Hits	P.Value
Hematopoietic cell lineage	5	0.0001
Complement and coagulation cascades	4	0.0010
Graft-versus-host disease	3	0.0010
Notch signalling pathway	4	0.0013
D-Glutamine and D-glutamate metabolism	1	0.0101
Pathways of neurodegeneration	**2**	**0.0102**

KEGG Pathways	Hits	P.Value
Oxidative phosphorylation	12	< 0.0001
Glutamatergic synapse	14	< 0.0001
Neurotrophin signalling pathway	4	0.0017
ABC transporters	6	0.0022
Pentose phosphate pathway	4	0.0022
Fructose and mannose metabolism	4	0.0031

KEGG Pathways	Hits	P.Value
Pyruvate metabolism	3	0.0022
Renin-angiotensin system	4	0.0027
Fatty acid elongation	2	0.0165
Neurotrophin signalling pathway	2	0.0176
Calcium signalling pathway	2	0.0471
Cysteine and methionine metabolism	2	0.0488

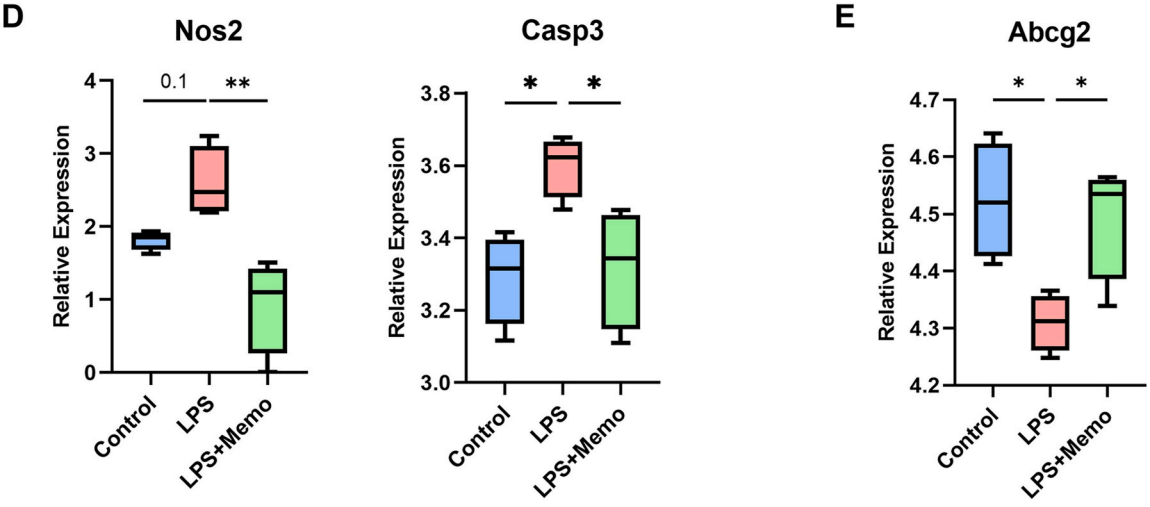

(caption on next page)

Fig. 5. Memophenol™ alters the transcriptional profile of the hippocampus. (A) Venn diagram displaying unique and overlapping significantly differentially expressed genes between pairwise analysis of the groups (B) Heatmap displaying the expression of the differentially expressed genes between groups. (C) Correlation network analysis illustrating significant correlations ($R > 0.5$; $p < 0.05$) between modulated circulatory metabolites—indoxyl sulfate, TMAO, *p*-cresol sulfate, and *p*-cresol glucuronide, which serve as the central nodes of the networks—and differentially expressed genes ($p < 0.05$) identified through RNA sequencing analysis. Metabolites are depicted as purple circles, forming the core of the network, while genes are shown as blue square nodes. Red lines represent positive correlations, and blue lines indicate negative correlations. Correlations are clustered to form coloured nodules, which are further analysed using KEGG pathway analysis to identify significantly modulated pathways related to gene expression and metabolite changes, highlighting potential mechanistic links between specific metabolites and gene expression changes in response to experimental conditions. (D) Relative expression of *Nos2* and *Casp3* genes which represent the two genes positively correlated with indoxyl sulfate in the pathways of neurodegeneration KEGG pathway. (E) Relative abundance of the indoxyl sulfate efflux transporter, *Abcg2*. (For interpretation of the references to colour in this figure legend, the reader is referred to the Web version of this article.)

modulation of the neurodegeneration-related gene pathway, indicating potential protective effects within the microbiota-gut-brain axis.

16S rRNA amplicon sequencing indicated significant modulation of the gut microbiome by LPS and Memophenol™ supplementation in comparison to control. At the genus level, Memophenol™ prevented the LPS-induced decrease of *Eubacterium_brachy_group* and *Romboutsia* and partially restored the abundance of *Muribaculum*, *Desulfovibrio* and the Firmicutes: Bacteridota ratio to control level. Gut bacterial changes were associated with the modulation of circulatory microbial-derived metabolites, most notably PCS, PCG, TMAO and IS concentrations. PCS and PCG concentrations were similar in LPS and control. However, Memophenol™ supplementation alongside LPS decreased concentrations of PCS and PCG reaching significantly lower than both the LPS and control group. These modulations negatively correlated with the abundance of *Lachnospiraceae A2*, *Butyricicoccus* and *Eubacterium brachy* bacterium, which were also significantly modulated between groups. *p*-Cresol is an exogenous uremic toxin primarily produced by the microbial conversion of tyrosine and phenylalanine in the colon. Due to its toxicity, *p*-cresol is further conjugated with sulfate or glucuronic acid by host cells such that it is almost entirely found as PCS or PCG in circulation and as such their concentrations are modulated by the gut microbiome (Liu et al., 2018; Shah et al., 2022). Aligning with our results, (poly)phenols have previously been found to increase *Eubacterium brachy* abundance (Wang et al., 2021). *Eubacterium brachy* metabolises the *p*-cresol precursor, phenylalanine, into phenylpropionate, cinnamate and phenylacetate (Hamid et al., 1994). Therefore, Memophenol™-induced increases may enhance phenylalanine metabolism through alternative pathways, shifting away from *p*-cresol production. Unlike high concentrations of PCS, low levels are insufficient to induce detrimental effects such as vascular permeability, oxidative stress and neuroinflammation (Sun et al., 2020; Tang et al., 2018), suggesting a potential protective effect of Memophenol™.

LPS significantly increased the abundance of *Desulfovibrio*, a bacterium that converts choline to TMA (a precursor to TMAO) via the *CutC* gene cluster (Craciun and Balskus, 2012). TMAO concentrations positively correlated with *Desulfovibrio* abundances suggesting a modulatory relationship between the two. Memophenol™ supplementation reduced *Desulfovibrio* in comparison to LPS ($p = 0.08$), aligning with previous studies suggesting that (poly)phenols reduce the abundance of the intestinal microbiota with the *CutC* gene (Jiang et al., 2024). This reduction may play a role in decreased circulatory TMAO concentrations, which is also supported by a reduction in TMA with Memophenol™ supplementation (Supplementary Table S5). Of note, LPS can also upregulate the expression of flavin-containing monooxygenase 3 (FMO3) (Xiao et al., 2022), an enzyme that catalyses the oxidation of TMA into TMAO in the liver. (Poly)phenols can reduce FMO3 expression, reducing TMAO in the blood (Jiang et al., 2024). As such, modulation of TMAO may be due to changes in gut microbial or biosynthetic metabolism.

The mechanism(s) by which TMAO affects human physiology remains poorly understood. High plasma TMAO levels (~5 μM) have been linked to gut microbial dysbiosis and systemic inflammation in patients with common variable immunodeficiency (Macpherson et al., 2020) and cardiovascular diseases (Zheng and He, 2022), though whether it is a cause or an effect remains unclear (Papandreou et al., 2020). While supraphysiological doses of TMAO have been associated with poor cardiovascular health, neuronal senescence, oxidative stress and mitochondrial dysfunction (Li et al., 2018; Papandreou et al., 2020), it is improbable for TMAO to naturally reach these concentrations, even under adverse conditions. Naturally increasing TMAO levels via the consumption of TMAO-rich foods, such as fish or seafood (Wang et al., 2022), or TMAO precursors, such as the choline-rich leafy vegetables (Van Parys et al., 2022), are considered part of a healthy diet. Protective roles have been observed for TMAO in rodent models of hypertension (Huc et al., 2018), glucose homeostasis (Dumas et al., 2017), atherosclerosis (Collins et al., 2016), non-alcoholic steatohepatitis (Zhao et al., 2019) and BBB integrity (Hoyles et al., 2021), with elevated levels acting as a compensatory mechanism to osmotic and hydrostatic stresses, processes that become elevated in inflammatory conditions such as those induced by LPS (Nakano et al., 2020). As such, it is plausible that TMAO modulation observed in LPS-induced inflammation is analogous to the increased levels of certain protective peptides, such as natriuretic peptide B, which serve as both markers of inflammatory stress and mediators of compensatory protective effects. This mechanism has been postulated to explain the strong positive correlation between TMAO and cardiovascular disease (Lundstrom and Racicot, 1983; Park et al., 2022). Our results may therefore indicate that altered TMAO levels are a byproduct of metabolic deviations, or an adaptive response aimed at mitigating the effects of LPS challenge. KEGG pathway analysis of TMAO-associated gene expression in the brain further emphasised processes associated with cellular homeostasis, redox balance, and protein synthesis (Jelleschitz et al., 2022; Minich, 2022; Stolwijk et al., 2020; Waterland, 2006), supporting the hypothesis that TMAO may play a role in buffering against inflammatory stress.

LPS was also associated with an increase in circulatory IS concentrations in comparison to control, which was mitigated by Memophenol™ supplementation. Modulation of IS was inversely correlated to the abundance of *Romboutsia*. *Romboutsia* has been associated with the functional kynB enzyme, which plays a central role within the kynurenine pathway of tryptophan metabolism (Vazquez-Medina et al., 2024). IS formed via the indole pathway, in which tryptophan is converted to indole by gut microbiota, which is subsequently absorbed, oxidised, and sulfated in the liver to produce IS. Decreases in *Romboutsia* under LPS may highlight a reduction in tryptophan metabolism via the kynurenine pathway, increasing tryptophan availability for IS production. Indeed, circulatory tryptophan concentrations were reduced in LPS and LPS + Memophenol™ in comparison to control. Memophenol™ supplementation significantly increased *Romboutsia,* abundance aligning with previous studies of the flavonoid-rich extract, Painong powder, in mice with colitis (Wang et al., 2022a). As a uremic toxin, IS has been found to accumulate in the blood of chronic kidney disease patients and is a predictor of overall cardiovascular morbidity/mortality (Hung et al., 2017). Renal impairment is associated with the accumulation of uremic toxins in circulation and the brain, leading to CNS dysfunction (Kelly and Rothwell, 2022). IS displays pro-inflammatory effects by acting on CNS and glial cells (Adesso et al., 2017, 2018) and has been proposed as a microbiota-derived metabolic surrogate for the development of CNS diseases (Sun et al., 2021).

Under LPS challenge, the brain displayed disrupted marginal location of the endothelial tight junction ZO-1, as well as decreased ZO-1

fluorescent intensity and mRNA expression, which was recovered by Memophenol™ supplementation. LPS has previously been used as an *in vivo* model of BBB disruption in mice, increasing BBB leakage and permeability, which coincided with decreased ZO-1 mRNA and protein expression (Gan et al., 2023; Hoyles et al., 2021). The modulation of ZO-1 mRNA levels negatively correlated with TMAO and IS concentrations, suggesting that decreases in these circulatory metabolites in the LPS + Memophenol™ group in comparison to LPS may be associated with increased ZO-1 expression. Interestingly, TMAO has previously been found to enhance BBB integrity and protect it from the effects of inflammation (Hoyles et al., 2021).

IS also negatively correlated with ZO-1 gene expression. Due to its ability to accumulate in the brain tissue and contribute to the disruption of neuronal damage and CNS homeostasis, IS can be considered a neurotoxin (Karbowska et al., 2020), and has previously been found to disrupt BBB permeability in rodent models of chronic kidney disease (Bobot et al., 2020). When investigating the underlying mechanism between ZO-1 and IS levels, KEGG pathway analysis highlighted a significant association between IS concentrations and genes associated with neurodegeneration, including increases in *Nos2* and *Casp3*, which were restored by Memophenol™ supplementation. NOS2 (or iNOS) is the inducible isoform of the mammalian nitric oxide synthases. Excessive production of NO by iNOS in the brain can cause neurotoxicity and BBB disruption (Toda et al., 2009). Transcriptional upregulation of iNOS, as well as increased production of 3-nitrotyrosine, appears to be characteristic of BBB breakdown following cerebral trauma (Nag et al., 2001). iNOS-deficient mice also display significantly reduced disruption of the BBB following experimental bacterial induction of meningitis compared to wild-type mice (Winkler et al., 2001). IS has previously been found *in vitro* to increase the production of iNOS in astrocytes and mixed glial cells, inducing conditions of oxidative stress (Adesso et al., 2017). Caspase-3 is also involved in ZO-1 disruption during cerebral ischemia (Zehendner et al., 2011). Inducing an inflammatory response of the human brain endothelial cells (BEC) hCMEC/D3 with cytokines induced caspase-3 activation, which even at low concentrations of cytokines, led to the redistribution of ZO-1 and VE-cadherin (Lopez-Ramirez et al., 2012). Inhibitors of caspase-3, as well as caspase-9, also partially blocked cytokine-induced disruption of ZO-1 and BEC permeability. IS has previously been found to significantly increase caspase-3 expression in mononuclear blood cells (Pieniazek et al., 2023) and mesangial cells (Cheng et al., 2020). Memophenol™ also restored expression of the IS efflux transporter *Abcg2* (also known as breast cancer resistance protein, BCRP) in the brain to control levels, which was decreased under LPS challenge (Takada et al., 2018), suggesting IS may be more efficiently expelled from the brain.

We recognise that our study has limitations, and further work will be required. Despite targeting some of the top metabolites currently associated with neuronal health (Connell et al., 2022), the gut microbiome is capable of directly and indirectly modifying a variety of metabolites which may contribute to the protective effects of Memophenol™. For example, short-chain fatty acids produced from the microbiota through the anaerobic fermentation of indigestible polysaccharides play a role in enhancing and protecting the BBB (Braniste et al., 2014; Hoyles et al., 2018; O'Riordan et al., 2022). Furthermore, despite our results outlining an association between IS and ZO-1 expression, as well as IS and *Casp3* and *Nos2*, further work will be required to establish the causality of the underlying mechanisms. This study also investigated the effect of Memophenol™ using only male mice. (Poly)phenol metabolism can be sexually dimorphic (Garrabou et al., 2022), and as such further studies investigating these results in females will be required.

Overall, our results suggest a novel neuroprotective effect of dietary Memophenol™ on the microbiota-gut-brain axis. Memophenol™ reduced concentrations of toxic microbial-derived metabolites, which was associated with moderate changes in gut microbiome composition, increased ZO-1 signalling and decreased *caspase-3* and *iNOS* gene expression. These results further highlight the interconnected nature of diet on the microbiota-gut-brain axis and brain health, providing further support for its use as a therapeutic intervention against chronic low-grade inflammation.

CRediT authorship contribution statement

Emily Connell: Writing – review & editing, Writing – original draft, Investigation, Formal analysis, Data curation. **Gwénaëlle Le Gall:** Writing – review & editing, Supervision, Investigation, Formal analysis, Data curation. **Simon McArthur:** Writing – review & editing, Supervision, Methodology, Formal analysis. **Leonie Lang:** Writing – review & editing, Formal analysis. **Bernadette Breeze:** Investigation, Writing – review & editing. **Matthew G. Pontifex:** Writing – review & editing, Writing – original draft, Methodology, Investigation. **Saber Sami:** Writing – review & editing, Supervision. **Line Pourtau:** Writing – review & editing, Resources. **David Gaudout:** Writing – review & editing, Resources. **Michael Müller:** Writing – review & editing, Supervision. **David Vauzour:** Writing – review & editing, Writing – original draft, Supervision, Funding acquisition, Conceptualization.

Declaration of competing interest

The authors declare the following financial interests/personal relationships which may be considered as potential competing interests:

David Vauzour reports financial support was provided by Activ'Inside. David Vauzour reports a relationship with Activ'Inside that includes: funding grants and travel reimbursement. David Gaudout has patent #WO/2017/072,219 licensed to Activ'Inside. If there are other authors, they declare that they have no known competing financial interests or personal relationships that could have appeared to influence the work reported in this paper.

Appendix A. Supplementary data

Supplementary data to this article can be found online at https://doi.org/10.1016/j.neuint.2024.105878.

Data availability

The 16 S rRNA gene sequence data have been deposited in the NCBI BioProject database (https://www.ncbi.nlm.nih.gov/bioproject/) under accession number PRJNA1127570.

References

Adesso, S., Magnus, T., Cuzzocrea, S., Campolo, M., Rissiek, B., Paciello, O., Autore, G., Pinto, A., Marzocco, S., 2017. Indoxyl sulfate affects glial function increasing oxidative stress and neuroinflammation in chronic kidney disease: interaction between astrocytes and microglia. Front. Pharmacol. 8, 370. https://doi.org/10.3389/fphar.2017.00370.

Adesso, S., Paterniti, I., Cuzzocrea, S., Fujioka, M., Autore, G., Magnus, T., Pinto, A., Marzocco, S., 2018. AST-120 reduces neuroinflammation induced by indoxyl sulfate in glial cells. J. Clin. Med. 7, 365. https://doi.org/10.3390/jcm7100365.

Bensalem, J., Dudonné, S., Etchamendy, N., Pellay, H., Amadieu, C., Gaudout, D., Dubreuil, S., Paradis, M.-E., Pomerleau, S., Capuron, L., Hudon, C., Layé, S., Desjardins, Y., Pallet, V., 2019. Polyphenols from grape and blueberry improve episodic memory in healthy elderly with lower level of memory performance: a bicentric double-blind, randomized, placebo-controlled clinical study. J. Gerontol. A .Biol. Sci. Med. Sci. 74, 996–1007. https://doi.org/10.1093/gerona/gly166.

Bensalem, J., Servant, L., Alfos, S., Gaudout, D., Layé, S., Lafenetre, P., Pallet, V., 2016. Dietary polyphenol supplementation prevents alterations of spatial navigation in middle-aged mice. Front. Behav. Neurosci. 10. https://doi.org/10.3389/fnbeh.2016.00009.

Bobot, M., Thomas, L., Moyon, A., Fernandez, S., McKay, N., Balasse, L., Garrigue, P., Brige, P., Chopinet, S., Poitevin, S., Cérini, C., Brunet, P., Dignat-George, F., Burtey, S., Guillet, B., Hache, G., 2020. Uremic toxic blood-brain barrier disruption mediated by AhR activation leads to cognitive impairment during experimental renal dysfunction. J. Am. Soc. Nephrol. 31, 1509–1521. https://doi.org/10.1681/ASN.2019070728.

Braniste, V., Al-Asmakh, M., Kowal, C., Anuar, F., Abbaspour, A., Tóth, M., Korecka, A., Bakocevic, N., Ng, L.G., Kundu, P., Gulyás, B., Halldin, C., Hultenby, K., Nilsson, H., Hebert, H., Volpe, B.T., Diamond, B., Pettersson, S., 2014. The gut microbiota

influences blood-brain barrier permeability in mice. Sci. Transl. Med. 6, 263ra158. https://doi.org/10.1126/scitranslmed.3009759.
Brentnall, M., Rodriguez-Menocal, L., De Guevara, R.L., Cepero, E., Boise, L.H., 2013. Caspase-9, caspase-3 and caspase-7 have distinct roles during intrinsic apoptosis. BMC Cell Biol. 14, 32. https://doi.org/10.1186/1471-2121-14-32.
Chakrabarti, A., Geurts, L., Hoyles, L., Iozzo, P., Kraneveld, A.D., La Fata, G., Miani, M., Patterson, E., Pot, B., Shortt, C., Vauzour, D., 2022. The microbiota-gut-brain axis: pathways to better brain health. Perspectives on what we know, what we need to investigate and how to put knowledge into practice. Cell. Mol. Life Sci. 79, 80. https://doi.org/10.1007/s00018-021-04060-w.
Cheng, T.-H., Ma, M.-C., Liao, M.-T., Zheng, C.-M., Lu, K.-C., Liao, C.-H., Hou, Y.-C., Liu, W.-C., Lu, C.-L., 2020. Indoxyl sulfate, a tubular toxin, contributes to the development of chronic kidney disease. Toxins 12, 684. https://doi.org/10.3390/toxins12110684.
Collins, H.L., Drazul-Schrader, D., Sulpizio, A.C., Koster, P.D., Williamson, Y., Adelman, S.J., Owen, K., Sanli, T., Bellamine, A., 2016. L-Carnitine intake and high trimethylamine N-oxide plasma levels correlate with low aortic lesions in ApoE(-/-) transgenic mice expressing CETP. Atherosclerosis 244, 29–37. https://doi.org/10.1016/j.atherosclerosis.2015.10.108.
Colton, C.A., Vitek, M.P., Wink, D.A., Xu, Q., Cantillana, V., Previti, M.L., Van Nostrand, W.E., Weinberg, J.B., Dawson, H., 2006. NO synthase 2 (NOS2) deletion promotes multiple pathologies in a mouse model of Alzheimer's disease. Proc. Natl. Acad. Sci. USA 103, 12867–12872. https://doi.org/10.1073/pnas.0601075103.
Connell, E., Le Gall, G., Pontifex, M.G., Sami, S., Cryan, J.F., Clarke, G., Müller, M., Vauzour, D., 2022. Microbial-derived metabolites as a risk factor of age-related cognitive decline and dementia. Mol. Neurodegener. 17, 43. https://doi.org/10.1186/s13024-022-00548-6.
Connell, E., Sami, S., Khondoker, M., Minihane, A.-M., Pontifex, M.G., Müller, M., McArthur, S., Gall, G.L., Vauzour, D., 2024. Circulatory dietary and gut-derived metabolites predict preclinical Alzheimer's disease. https://doi.org/10.1101/2024.05.10.24307050.
Craciun, S., Balskus, E.P., 2012. Microbial conversion of choline to trimethylamine requires a glycyl radical enzyme. Proc. Natl. Acad. Sci. U. S. A. 109, 21307–21312. https://doi.org/10.1073/pnas.1215689109.
Dal-Pan, A., Dudonné, S., Bourassa, P., Bourdoulous, M., Tremblay, C., Desjardins, Y., Calon, F., Neurophenols consortium, 2017. Cognitive-enhancing effects of a polyphenols-rich extract from fruits without changes in neuropathology in an animal model of Alzheimer's disease. J. Alzheimers. Dis. 55, 115–135. https://doi.org/10.3233/JAD-160281.
Del Rio, D., Rodriguez-Mateos, A., Spencer, J.P.E., Tognolini, M., Borges, G., Crozier, A., 2013. Dietary (poly)phenolics in human health: structures, bioavailability, and evidence of protective effects against chronic diseases. Antioxidants Redox Signal. 18, 1818–1892. https://doi.org/10.1089/ars.2012.4581.
Dumas, M.-E., Rothwell, A.R., Hoyles, L., Aranias, T., Chilloux, J., Calderari, S., Noll, E. M., Péan, N., Boulangé, C.L., Blancher, C., Barton, R.H., Gu, Q., Fearnside, J.F., Deshayes, C., Hue, C., Scott, J., Nicholson, J.K., Gauguier, D., 2017. Microbial-host Co-metabolites are prodromal markers predicting phenotypic heterogeneity in behavior, obesity, and impaired glucose tolerance. Cell Rep. 20, 136–148. https://doi.org/10.1016/j.celrep.2017.06.039.
Gan, N., Zhou, Y., Li, J., Wang, A., Cao, Y., 2023. Propofol suppresses LPS-induced BBB damage by regulating miR-130a-5p/ZO-1 Axis. Mol. Biotechnol. https://doi.org/10.1007/s12033-023-00835-7.
Garrabou, G., García-García, F.J., Presmanes, R.E., Feu, M., Chiva-Blanch, G., 2022. Relevance of sex-differenced analyses in bioenergetics and nutritional studies. Front. Nutr. 9. https://doi.org/10.3389/fnut.2022.936929.
Garrido, J., Borges, F., 2013. Wine and grape polyphenols — a chemical perspective. Food Res. Int. 54, 1844–1858. https://doi.org/10.1016/j.foodres.2013.08.002.
Hamid, M.A., Iwaku, M., Hoshino, E., 1994. The metabolism of phenylalanine and leucine by a cell suspension of Eubacterium brachy and the effects of metronidazole on metabolism. Arch. Oral Biol. 39, 967–972. https://doi.org/10.1016/0003-9969(94)90080-9.
Hoyles, L., Pontifex, M.G., Rodriguez-Ramiro, I., Anis-Alavi, M.A., Jelane, K.S., Snelling, T., Solito, E., Fonseca, S., Carvalho, A.L., Carding, S.R., Müller, M., Glen, R. C., Vauzour, D., McArthur, S., 2021. Regulation of blood-brain barrier integrity by microbiome-associated methylamines and cognition by trimethylamine N-oxide. Microbiome 9, 235. https://doi.org/10.1186/s40168-021-01181-z.
Hoyles, L., Snelling, T., Umlai, U.-K., Nicholson, J.K., Carding, S.R., Glen, R.C., McArthur, S., 2018. Microbiome–host systems interactions: protective effects of propionate upon the blood–brain barrier. Microbiome 6, 55. https://doi.org/10.1186/s40168-018-0439-y.
Huc, T., Drapala, A., Gawrys, M., Konop, M., Bielinska, K., Zaorska, E., Samborowska, E., Wyczalkowska-Tomasik, A., Pączek, L., Dadlez, M., Ufnal, M., 2018. Chronic, low-dose TMAO treatment reduces diastolic dysfunction and heart fibrosis in hypertensive rats. Am. J. Physiol. Heart Circ. Physiol. 315, H1805–H1820. https://doi.org/10.1152/ajpheart.00536.2018.
Hung, S.-C., Kuo, K.-L., Wu, C.-C., Tarng, D.-C., 2017. Indoxyl sulfate: a novel cardiovascular risk factor in chronic kidney disease. J. Am. Heart Assoc.: Cardiovascular and Cerebrovascular Disease. 6. https://doi.org/10.1161/JAHA.116.005022.
Iqbal, I., Wilairatana, P., Saqib, F., Nasir, B., Wahid, M., Latif, M.F., Iqbal, A., Naz, R., Mubarak, M.S., 2023. Plant polyphenols and their potential benefits on cardiovascular health: a review. Molecules 28. https://doi.org/10.3390/molecules28176403.
Jelleschitz, J., Zhang, Y., Grune, T., Chen, W., Zhao, Y., Jia, M., Wang, Y., Liu, Z., Höhn, A., 2022. Methionine restriction - association with redox homeostasis and implications on aging and diseases. Redox Biol. 57, 102464. https://doi.org/10.1016/j.redox.2022.102464.
Jiang, C., Wang, S., Wang, Y., Wang, K., Huang, C., Gao, F., peng Hu, H., Deng, Y., Zhang, W., Zheng, J., Huang, J., Li, Y., 2024. Polyphenols from hickory nut reduce the occurrence of atherosclerosis in mice by improving intestinal microbiota and inhibiting trimethylamine N-oxide production. Phytomedicine 128, 155349. https://doi.org/10.1016/j.phymed.2024.155349.
Karbowska, M., Hermanowicz, J.M., Tankiewicz-Kwedlo, A., Kalaska, B., Kaminski, T.W., Nosek, K., Wisniewska, R.J., Pawlak, D., 2020. Neurobehavioral effects of uremic toxin–indoxyl sulfate in the rat model. Sci. Rep. 10, 9483. https://doi.org/10.1038/s41598-020-66421-y.
Kelly, D.M., Rothwell, P.M., 2022. Disentangling the relationship between chronic kidney disease and cognitive disorders. Front. Neurol. 13. https://doi.org/10.3389/fneur.2022.830064.
Krikorian, R., Nash, T.A., Shidler, M.D., Shukitt-Hale, B., Joseph, J.A., 2010a. Concord grape juice supplementation improves memory function in older adults with mild cognitive impairment. Br. J. Nutr. 103, 730–734. https://doi.org/10.1017/S0007114509992364.
Krikorian, R., Shidler, M.D., Nash, T.A., Kalt, W., Vinqvist-Tymchuk, M.R., Shukitt-Hale, B., Joseph, J.A., 2010b. Blueberry supplementation improves memory in older adults. J. Agric. Food Chem. 58, 3996–4000. https://doi.org/10.1021/jf9029332.
Láng, L., McArthur, S., Lazar, A.S., Pourtau, L., Gaudout, D., Pontifex, M.G., Müller, M., Vauzour, D., 2024. Dietary (Poly)phenols and the gut–brain Axis in ageing. Nutrients 16, 1500. https://doi.org/10.3390/nu16101500.
Li, D., Ke, Y., Zhan, R., Liu, C., Zhao, M., Zeng, A., Shi, X., Ji, L., Cheng, S., Pan, B., Zheng, L., Hong, H., 2018. Trimethylamine-N-oxide promotes brain aging and cognitive impairment in mice. Aging Cell 17, e12768. https://doi.org/10.1111/acel.12768.
Liao, Y., Smyth, G.K., Shi, W., 2014. featureCounts: an efficient general purpose program for assigning sequence reads to genomic features. Bioinformatics 30, 923–930. https://doi.org/10.1093/bioinformatics/btt656.
Liu, W.-C., Tomino, Y., Lu, K.-C., 2018. Impacts of indoxyl sulfate and p-cresol sulfate on chronic kidney disease and mitigating effects of AST-120. Toxins. 10, 367. https://doi.org/10.3390/toxins10090367.
Lopez-Ramirez, M.A., Fischer, R., Torres-Badillo, C.C., Davies, H.A., Logan, K., Pfizenmaier, K., Male, D.K., Sharrack, B., Romero, I.A., 2012. Role of caspases in cytokine-induced barrier breakdown in human brain endothelial cells. J. Immunol. 189, 3130–3139. https://doi.org/10.4049/jimmunol.1103460.
Lopresti, A.L., Smith, S.J., Pouchieu, C., Pourtau, L., Gaudout, D., Pallet, V., Drummond, P.D., 2023. Effects of a polyphenol-rich grape and blueberry extract (Memophenol™) on cognitive function in older adults with mild cognitive impairment: a randomized, double-blind, placebo-controlled study. Front. Psychol. 14, 1144231. https://doi.org/10.3389/fpsyg.2023.1144231.
Lundstrom, R.C., Racicot, L.D., 1983. Gas chromatographic determination of dimethylamine and trimethylamine in seafoods. J. Assoc. Off. Anal. Chem. 66, 1158–1163.
Ma, L., Sun, Z., Zeng, Y., Luo, M., Yang, J., 2018. Molecular mechanism and health role of functional ingredients in blueberry for chronic disease in human beings. Int. J. Mol. Sci. 19, 2785. https://doi.org/10.3390/ijms19092785.
Macpherson, M.E., Hov, J.R., Ueland, T., Dahl, T.B., Kummen, M., Otterdal, K., Holm, K., Berge, R.K., Mollnes, T.E., Trøseid, M., Halvorsen, B., Aukrust, P., Fevang, B., Jørgensen, S.F., 2020. Gut microbiota-dependent trimethylamine N-oxide associates with inflammation in common variable immunodeficiency. Front. Immunol. 11, 574500. https://doi.org/10.3389/fimmu.2020.574500.
Minich, W.B., 2022. Selenium metabolism and biosynthesis of selenoproteins in the human body. Biochemistry (Mosc.) 87, S168–S177. https://doi.org/10.1134/S0006297922140139.
Mithul Aravind, S., Wichienchot, S., Tsao, R., Ramakrishnan, S., Chakkaravarthi, S., 2021. Role of dietary polyphenols on gut microbiota, their metabolites and health benefits. Food Res. Int. 142, 110189. https://doi.org/10.1016/j.foodres.2021.110189.
Moles, L., Otaegui, D., 2020. The impact of diet on microbiota evolution and human health. Is diet an adequate tool for microbiota modulation? Nutrients 12, 1654. https://doi.org/10.3390/nu12061654.
Moreno-Torres, M., García-Llorens, G., Moro, E., Méndez, R., Quintás, G., Castell, J.V., 2021. Factors that influence the quality of metabolomics data in in vitro cell toxicity studies: a systematic survey. Sci. Rep. 11, 22119. https://doi.org/10.1038/s41598-021-01652-1.
Mortazavi, A., Williams, B.A., McCue, K., Schaeffer, L., Wold, B., 2008. Mapping and quantifying mammalian transcriptomes by RNA-Seq. Nat. Methods. 5, 621–628. https://doi.org/10.1038/nmeth.1226.
Mutha, R.E., Tatiya, A.U., Surana, S.J., 2021. Flavonoids as natural phenolic compounds and their role in therapeutics: an overview. Futur. J. Pharm. Sci. 7, 25. https://doi.org/10.1186/s43094-020-00161-8.
Nag, S., Picard, P., Stewart, D.J., 2001. Expression of nitric oxide synthases and nitrotyrosine during blood-brain barrier breakdown and repair after cold injury. Lab. Invest. 81, 41–49. https://doi.org/10.1038/labinvest.3780210.
Nair, A.B., Jacob, S., 2016. A simple practice guide for dose conversion between animals and human. J. Basic Clin. Pharm. 7, 27–31. https://doi.org/10.4103/0976-0105.177703.
Nakano, D., Kitada, K., Wan, N., Zhang, Y., Wiig, H., Wararat, K., Yanagita, M., Lee, S., Jia, L., Titze, J.M., Nishiyama, A., 2020. Lipopolysaccharide induces filtrate leakage from renal tubular lumina into the interstitial space via a proximal tubular Toll-like receptor 4–dependent pathway and limits sensitivity to fluid therapy in mice. Kidney Int. 97, 904–912. https://doi.org/10.1016/j.kint.2019.11.024.

Ni, Y., Yu, G., Chen, H., Deng, Y., Wells, P.M., Steves, C.J., Ju, F., Fu, J., 2020. M2IA: a web server for microbiome and metabolome integrative analysis. Bioinformatics 36, 3493–3498. https://doi.org/10.1093/bioinformatics/btaa188.

O'Riordan, K.J., Collins, M.K., Moloney, G.M., Knox, E.G., Aburto, M.R., Fülling, C., Morley, S.J., Clarke, G., Schellekens, H., Cryan, J.F., 2022. Short chain fatty acids: microbial metabolites for gut-brain axis signalling. Mol. Cell. Endocrinol. 546, 111572. https://doi.org/10.1016/j.mce.2022.111572.

Pang, Z., Zhou, G., Ewald, J., Chang, L., Hacariz, O., Basu, N., Xia, J., 2022. Using MetaboAnalyst 5.0 for LC–HRMS spectra processing, multi-omics integration and covariate adjustment of global metabolomics data. Nat. Protoc. 17, 1735–1761. https://doi.org/10.1038/s41596-022-00710-w.

Papandreou, C., Moré, M., Bellamine, A., 2020. Trimethylamine N-oxide in relation to cardiometabolic health—cause or effect? Nutrients 12, 1330. https://doi.org/10.3390/nu12051330.

Park, G.-H., Cho, J.-H., Lee, D., Kim, Y., 2022. Association between seafood intake and cardiovascular disease in south Korean adults: a community-based prospective cohort study. Nutrients 14, 4864. https://doi.org/10.3390/nu14224864.

Parkhomchuk, D., Borodina, T., Amstislavskiy, V., Banaru, M., Hallen, L., Krobitsch, S., Lehrach, H., Soldatov, A., 2009. Transcriptome analysis by strand-specific sequencing of complementary DNA. Nucleic Acids Res. 37, e123. https://doi.org/10.1093/nar/gkp596.

Philip, P., Sagaspe, P., Taillard, J., Mandon, C., Constans, J., Pourtau, L., Pouchieu, C., Angelino, D., Mena, P., Martini, D., Del Rio, D., Vauzour, D., 2019. Acute intake of a grape and blueberry polyphenol-rich extract ameliorates cognitive performance in healthy young adults during a sustained cognitive effort. Antioxidants. 8, 650. https://doi.org/10.3390/antiox8120650.

Pieniazek, A., Bernasinska-Slomczewska, J., Hikisz, P., 2023. Indoxyl sulfate induces apoptosis in mononuclear blood cells via mitochondrial pathway. Sci. Rep. 13, 14044. https://doi.org/10.1038/s41598-023-40824-z.

Pontifex, M.G., Connell, E., Gall, G.L., Pourtau, L., Gaudout, D., Angeloni, C., Zallocco, L., Ronci, M., Giusti, L., Müller, M., Vauzour, D., 2022. Saffron extract (Safr'Inside™) improves anxiety related behaviour in a mouse model of low-grade inflammation through the modulation of the microbiota and gut derived metabolites. Food Funct. 13, 12219–12233. https://doi.org/10.1039/D2FO02739A.

Quast, C., Pruesse, E., Yilmaz, P., Gerken, J., Schweer, T., Yarza, P., Peplies, J., Glöckner, F.O., 2013. The SILVA ribosomal RNA gene database project: improved data processing and web-based tools. Nucleic Acids Res. 41, D590–D596. https://doi.org/10.1093/nar/gks1219.

Ramis, M.R., Sarubbo, F., Tejada, S., Jiménez, M., Esteban, S., Miralles, A., Moranta, D., 2020. Chronic polyphenon-60 or catechin treatments increase brain monoamines syntheses and hippocampal SIRT1 LEVELS improving cognition in aged rats. Nutrients 12, 326. https://doi.org/10.3390/nu12020326.

Rendeiro, C., Vauzour, D., Kean, R.J., Butler, L.T., Rattray, M., Spencer, J.P.E., Williams, C.M., 2012. Blueberry supplementation induces spatial memory improvements and region-specific regulation of hippocampal BDNF mRNA expression in young rats. Psychopharmacology 223, 319–330. https://doi.org/10.1007/s00213-012-2719-8.

Romo-Vaquero, M., Fernández-Villalba, E., Gil-Martinez, A.-L., Cuenca-Bermejo, L., Espín, J.C., Herrero, M.T., Selma, M.V., 2022. Urolithins: potential biomarkers of gut dysbiosis and disease stage in Parkinson's patients. Food Funct. 13, 6306–6316. https://doi.org/10.1039/d2fo00552b.

Sarkaki, A., Farbood, Y., Badavi, M., 2007. The effect of grape seed extract (GSE) on spatial memory in aged male rats. Pakistan J. Med. Sci. 23, 561–565.

Sert, N.P. du, Hurst, V., Ahluwalia, A., Alam, S., Avey, M.T., Baker, M., Browne, W.J., Clark, A., Cuthill, I.C., Dirnagl, U., Emerson, M., Garner, P., Holgate, S.T., Howells, D.W., Karp, N.A., Lazic, S.E., Lidster, K., MacCallum, C.J., Macleod, M., Pearl, E.J., Petersen, O.H., Rawle, F., Reynolds, P., Rooney, K., Sena, E.S., Silberberg, S.D., Steckler, T., Würbel, H., 2020. The ARRIVE guidelines 2.0: updated guidelines for reporting animal research. PLoS Biol. 18, e3000410. https://doi.org/10.1371/journal.pbio.3000410.

Shah, S.N., Knausenberger, T.B.-A., Connell, E., Gall, G.L., Hardy, T.A.J., Randall, D.W., McCafferty, K., Yaqoob, M.M., Solito, E., Müller, M., Stachulski, A.V., Glen, R.C., Vauzour, D., Hoyles, L., McArthur, S., 2022. Cerebrovascular damage caused by the gut microbe-derived uraemic toxin p-cresol sulfate is prevented by blockade of the epidermal growth factor receptor. https://doi.org/10.1101/2022.11.12.516113.

Shukitt-Hale, B., Carey, A., Simon, L., Mark, D.A., Joseph, J.A., 2006. Effects of Concord grape juice on cognitive and motor deficits in aging. Nutrition 22, 295–302. https://doi.org/10.1016/j.nut.2005.07.016.

Singh, M., Arseneault, M., Sanderson, T., Murthy, V., Ramassamy, C., 2008. Challenges for research on polyphenols from foods in Alzheimer's disease: bioavailability, metabolism, and cellular and molecular mechanisms. J. Agric. Food Chem. 56, 4855–4873. https://doi.org/10.1021/jf0735073.

Song, C., Zhang, Y., Cheng, L., Shi, M., Li, X., Zhang, L., Zhao, H., 2021. Tea polyphenols ameliorates memory decline in aging model rats by inhibiting brain TLR4/NF-κB inflammatory signaling pathway caused by intestinal flora dysbiosis. Exp. Gerontol. 153, 111476. https://doi.org/10.1016/j.exger.2021.111476.

Stolwijk, J.M., Garje, R., Sieren, J.C., Buettner, G.R., Zakharia, Y., 2020. Understanding the redox biology of selenium in the search of targeted cancer therapies. Antioxidants. 9, 420. https://doi.org/10.3390/antiox9050420.

Sun, C.-Y., Li, J.-R., Wang, Y.-Y., Lin, S.-Y., Ou, Y.-C., Lin, C.-J., Wang, J.-D., Liao, S.-L., Chen, C.-J., 2021. Indoxyl sulfate caused behavioral abnormality and neurodegeneration in mice with unilateral nephrectomy. Aging (Albany NY) 13, 6681–6701. https://doi.org/10.18632/aging.202523.

Sun, C.-Y., Li, J.-R., Wang, Y.-Y., Lin, S.-Y., Ou, Y.-C., Lin, C.-J., Wang, J.-D., Liao, S.-L., Chen, C.-J., 2020. p-Cresol sulfate caused behavior disorders and neurodegeneration in mice with unilateral nephrectomy involving oxidative stress and neuroinflammation. Int. J. Mol. Sci. 21, E6687. https://doi.org/10.3390/ijms21186687.

Takada, T., Yamamoto, T., Matsuo, H., Tan, J.K., Ooyama, K., Sakiyama, M., Miyata, H., Yamanashi, Y., Toyoda, Y., Higashino, T., Nakayama, A., Nakashima, A., Shinomiya, N., Ichida, K., Ooyama, H., Fujimori, S., Suzuki, H., 2018. Identification of ABCG2 as an exporter of uremic toxin indoxyl sulfate in mice and as a crucial factor influencing CKD progression. Sci. Rep. 8, 11147. https://doi.org/10.1038/s41598-018-29208-w.

Tang, W.-H., Wang, C.-P., Yu, T.-H., Tai, P.-Y., Liang, S.-S., Hung, W.-C., Wu, C.-C., Huang, S.-H., Lee, Y.-J., Chen, S.-C., 2018. Protein-bounded uremic toxin p-cresylsulfate induces vascular permeability alternations. Histochem. Cell Biol. 149, 607–617. https://doi.org/10.1007/s00418-018-1662-0.

Toda, N., Ayajiki, K., Okamura, T., 2009. Cerebral blood flow regulation by nitric oxide: recent advances. Pharmacol. Rev. 61, 62–97. https://doi.org/10.1124/pr.108.000547.

Troppmann, L., Gray-Donald, K., Johns, T., 2002. Supplement use: is there any nutritional benefit? J. Am. Diet Assoc. 102, 818–825. https://doi.org/10.1016/s0002-8223(02)90183-5.

Van Parys, A., Brække, M.S., Karlsson, T., Vinknes, K.J., Tell, G.S., Haugsgjerd, T.R., Ueland, P.M., Øyen, J., Dierkes, J., Nygård, O., Lysne, V., 2022. Assessment of dietary choline intake, contributing food items, and associations with one-carbon and lipid metabolites in middle-aged and elderly adults: the hordaland health study. J. Nutr. 152, 513–524. https://doi.org/10.1093/jn/nxab367.

Vazquez-Medina, A., Rodriguez-Trujillo, N., Ayuso-Rodriguez, K., Marini-Martinez, F., Angeli-Morales, R., Caussade-Silvestrini, G., Godoy-Vitorino, F., Chorna, N., 2024. Exploring the interplay between running exercises, microbial diversity, and tryptophan metabolism along the microbiota-gut-brain axis. Front. Microbiol. 15. https://doi.org/10.3389/fmicb.2024.1326584.

Wang, F., Zhao, C., Yang, M., Zhang, Lin, Wei, R., Meng, K., Bao, Y., Zhang, Lina, Zheng, J., 2021. Four citrus flavanones exert atherosclerosis alleviation effects in ApoE−/− mice via different metabolic and signaling pathways. J. Agric. Food Chem. 69, 5226–5237. https://doi.org/10.1021/acs.jafc.1c01463.

Wang, K., Guo, J., Chang, X., Gui, S., 2022. Painong-San extract alleviates dextran sulfate sodium-induced colitis in mice by modulating gut microbiota, restoring intestinal barrier function and attenuating TLR4/NF-κB signaling cascades. J. Pharm. Biomed. Anal. 209, 114529. https://doi.org/10.1016/j.jpba.2021.114529.

Wang, Q., Garrity, G.M., Tiedje, J.M., Cole, J.R., 2007. Naive Bayesian classifier for rapid assignment of rRNA sequences into the new bacterial taxonomy. Appl. Environ. Microbiol. 73, 5261–5267. https://doi.org/10.1128/AEM.00062-07.

Wang, Z., Tang, W.H.W., O'Connell, T., Garcia, E., Jeyarajah, E.J., Li, X.S., Jia, X., Weeks, T.L., Hazen, S.L., 2022. Circulating trimethylamine N-oxide levels following fish or seafood consumption. Eur. J. Nutr. 61, 2357–2364. https://doi.org/10.1007/s00394-022-02803-4.

Waterland, R.A., 2006. Assessing the effects of high methionine intake on DNA Methylation 12. J. Nutr. 136, 1706S–1710S. https://doi.org/10.1093/jn/136.6.1706S.

Winkler, F., Koedel, U., Kastenbauer, S., Pfister, H.W., 2001. Differential expression of nitric oxide synthases in bacterial meningitis: role of the inducible isoform for blood-brain barrier breakdown. J. Infect. Dis. 183, 1749–1759. https://doi.org/10.1086/320730.

Xiao, L., Huang, L., Zhou, X., Zhao, D., Wang, Y., Min, H., Song, S., Sun, W., Gao, Q., Hu, Q., Xie, S., 2022. Experimental periodontitis deteriorated atherosclerosis associated with trimethylamine N-oxide metabolism in mice. Front. Cell. Infect. Microbiol. 11. https://doi.org/10.3389/fcimb.2021.820535.

Zehendner, C.M., Librizzi, L., de Curtis, M., Kuhlmann, C.R.W., Luhmann, H.J., 2011. Caspase-3 contributes to ZO-1 and Cl-5 tight-junction disruption in rapid anoxic neurovascular unit damage. PLoS One 6, e16760. https://doi.org/10.1371/journal.pone.0016760.

Zhao, Z.-H., Xin, F.-Z., Zhou, D., Xue, Y.-Q., Liu, X.-L., Yang, R.-X., Pan, Q., Fan, J.-G., 2019. Trimethylamine N-oxide attenuates high-fat high-cholesterol diet-induced steatohepatitis by reducing hepatic cholesterol overload in rats. World J. Gastroenterol. 25, 2450–2462. https://doi.org/10.3748/wjg.v25.i20.2450.

Zheng, Y., He, J.-Q., 2022. Pathogenic mechanisms of trimethylamine N-Oxide-induced atherosclerosis and cardiomyopathy. Curr. Vasc. Pharmacol. 20, 29. https://doi.org/10.2174/1570161119666210812152802.

Zhou, G., Ewald, J., Xia, J., 2021. OmicsAnalyst: a comprehensive web-based platform for visual analytics of multi-omics data. Nucleic Acids Res. 49, W476–W482. https://doi.org/10.1093/nar/gkab394.